

Data-driven discovery of quasiperiodically driven dynamics

Shakib Mustavee, Suddhasattwa Das, Shaurya Agarwal

Abstract

Quasiperiodically driven dynamical systems are nonlinear systems which are driven by some periodic source with multiple base-frequencies. Such systems abound in nature, and are present in data collected from sources such as astronomy and traffic data. We present a completely data-driven procedure which reconstructs the dynamics into two components - the driving quasiperiodic source with generating frequencies; and the driven nonlinear dynamics. Unlike conventional methods based on DMD or neural networks, we use kernel based methods. We utilize our structural assumption on the dynamics to conceptually separate the dynamics into a quasiperiodic and nonlinear part. We then use a kernel based Harmonic analysis and kernel based interpolation technique in a combined manner to discover these two parts. Our technique is shown to provide accurate reconstructions and frequency identification for datasets collected from three real world systems.

Keywords. Quasiperiodicity, Koopman operator, Koopman eigenfunctions, skew-product dynamics

Mathematics Subject Classification 2020. 37N30, 37M99, 37M10

1 Introduction.

Our goal is to present a class of dynamical systems which we call *quasiperiodically driven dynamics*, stated formally as the map

$$F : \mathbb{T}^d \times \mathcal{M} \rightarrow \mathbb{T}^d \times \mathcal{M}, \quad \begin{pmatrix} \theta_{n+1} \\ x_{n+1} \end{pmatrix} = F \begin{pmatrix} \theta_n \\ x_n \end{pmatrix} = \begin{pmatrix} \theta_n + \rho \bmod \mathbb{T}^d \\ (x_n, \theta_n) \end{pmatrix}, \quad (1)$$

Here the variable θ is an angular coordinate on a d -dimensional torus \mathbb{T}^d , x is a point in some abstract or unknown manifold \mathcal{M} , and $g : \mathbb{T}^d \times \mathcal{M} \rightarrow \mathcal{M}$ is some nonlinear function. θ represents the *phase* of a driving quasiperiodic rotation [1, 2], and the vector ρ is called the *rotation vector* [e.g. 3, 4]. ρ represents the angular increments at each step for each of the coordinates of θ . Thus (1) is a *one-way coupled* or *skew-product* dynamical system on the space $\Omega := \mathbb{T}^d \times \mathcal{M}$. This model of a dynamical system captures the essence of many physical systems which are influenced or driven by an external, quasiperiodic phenomena. Some examples are models for physiological activities, astronomical data [5], traffic dynamics [6, 7], climate data [8, 9], and physical flows on periodic domains [10, 11, 12]. This autonomous periodic phenomenon could be seasonal, weekly or diurnal cycles, or geographic location. If the underlying system arises from a continuous time system by taking samples at intervals Δt , then $\rho = \Delta t \omega$ for some angular frequency vector ω . This model can be summarized as the formal assumption :

Assumption 1. *There is a dynamical system of the form (1) for some $\rho \in \mathbb{T}^d$, m -dimensional manifold \mathcal{M} , and a differentiable function $g : \mathbb{T}^d \times \mathcal{M} \rightarrow \mathcal{M}$. This dynamics has an invariant probability measure μ with compact support $X \subseteq \mathbb{T}^d \times \mathcal{M}$.*

All dynamical systems which can be studied through experiments or measurements must have bounded trajectories. And any dynamical system with bounded trajectories must have at least one invariant probability measure. Let ν be the push forward of μ onto \mathcal{M} , defined for every open subset A of \mathcal{M} as

$$\nu(A) := \mu \{(\theta, x) : \theta \in \mathbb{T}^d, x \in A\},$$

It can be shown that μ is in fact the product of the Lebesgue volume measure on the torus, and this measure ν . To further uncover the structure of the dynamics in (1), consider the following averages

$$g_{per}(\theta) := \int g(\theta, x) d\nu(x), \quad \forall \theta \in \mathbb{T}^d. \quad (2)$$

As a result one can rewrite g as

$$g(\theta, x) = g_{per}(\theta) + g_{chaos}(\theta, x), \quad \forall \theta \in \mathbb{T}^d, \forall x \in \mathcal{M}. \quad (3)$$

The coordinate θ represents a periodically changing *phase* of an autonomous dynamical system $\theta_{n+1} = \theta_n + \rho \bmod 2\pi$. The coordinate x is to be interpreted as a set of variables, driven by θ and also simultaneously by its own current value. By virtue of (2), the component g_{chaos} has zero-mean with respect to x . The system will be said to have *constant sensitivity* if the following holds :

Assumption 2 (Constant sensitivity). *The partial derivative of the function g (from (1)) with respect to x is independent of θ . In other words*

$$\frac{\partial}{\partial \theta} \frac{\partial}{\partial x} g \equiv 0.$$

Assumption 2 simplifies (3) and thus (1) into the following form :

$$\begin{aligned} \theta_{n+1} &= \theta_n + \Delta t \bar{\omega} \bmod 2\pi \\ x_{n+1} &= g_{per}(\theta_n) + g_{chaos}(x_n) \end{aligned} \quad (4)$$

Equation (4) interprets the action of g on x as a zero-mean function g_{chaos} of x , along with a mean value dependent on the phase θ via the function g_{per} . The dynamics in the variable x takes the format of additively forced dynamical systems, studied in various contexts [e.g. 13, 14, 15].

Goal. Our is to develop a purely data-driven technique that constructs a model of the format of (4), to fit to data. Thus the task is to find (i) the *quasiperiodicity dimension* d and the rotation vector ω ; and the functions (ii) g_{per} and (iii) g_{chaos} . Our techniques rely on the Koopman operator theoretic formulation of the dynamics, and are implemented using kernel-based techniques for learning and frequency analysis [16]. See Figures 1, 2 and 3 for illustrations of the results of applying our methods to various real world systems. The numerical techniques we use are based on principles from ergodic theory [16] and kernel-based learning theory [17, 18, e.g.]. As a result our reconstruction provably converges to the true dynamics, in a general situation precisely defined by a set of formal Assumptions. We next describe the conditions of our data-driven framework.

Data-driven framework. In our approach, the functions and spaces in Assumption 1 will be assumed to be unknown. The only information about the system will be through a collection of k observations / measurements, represented collectively as a map $Y : \Omega \rightarrow \mathbb{R}^k$. More precisely :

Assumption 3. *There is an unknown continuous function / observation $Y : \Omega \rightarrow \mathbb{R}^k$, which is possibly a low-dimensional / partial observation of the dynamics. The data available for processing is the sequence of k -dimensional data point $\{y_n := Y(\theta_n, x_n) : n = 0, 1, 2, \dots\}$, where (θ_n, x_n) is a trajectory of the dynamics in (1) under F .*

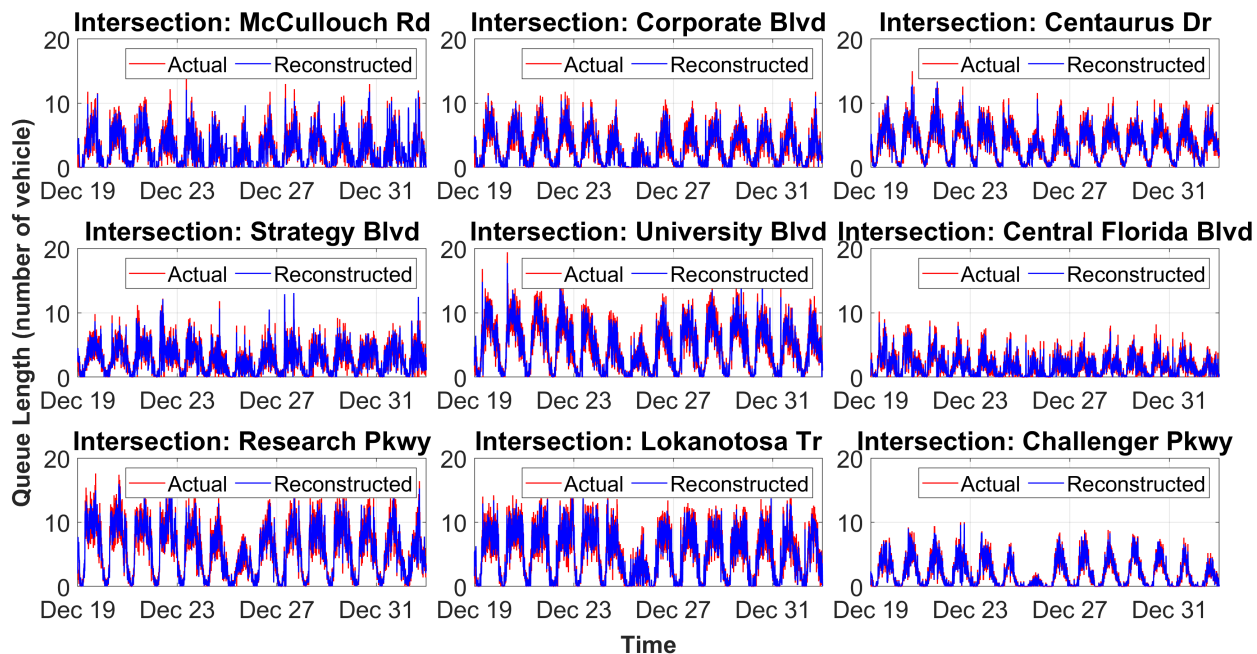


Figure 1: Traffic intersection dynamics as a quasiperiodically driven system. The blue curves in each of the 9 panels are traffic queue-length data collected at 9 different intersections on the Alafaya freeway of the Florida State road system. These curves carry the effects of stochastic, chaotic as well as periodic components of the traffic system. The red curve is the output obtained from simulating a numerically constructed dynamical system described in (15). The close match between the two curves, in terms of their periodicities, fluctuations and absolute error, highlights the theoretical and numerical contributions of our work. We axiomatically define a class of dynamics called *quasiperiodically driven* dynamics, via Equations (1), (4), and formal Assumptions 1 and 2. We develop kernel based learning techniques in Section 4, and show that in a purely data-drive setting described in Assumption 3, the results of our techniques converge to the true dynamical system. Our techniques rely heavily on ergodic theory, and RKHS theory, described in Sections 2 and 3 respectively. See Section 5 for a full description of the intersection dynamics, as well as three other physical systems. Also see Figures 2 and 3 for a similar analysis of other real world dynamical systems as quasiperiodically driven dynamics.

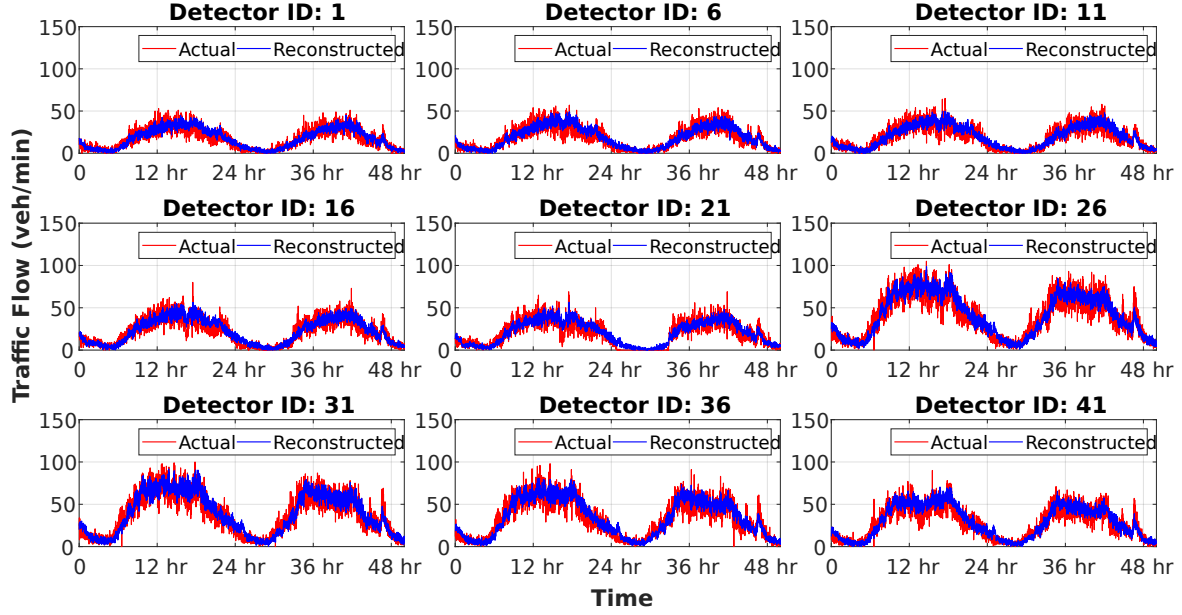


Figure 2: Highway traffic flow as a quasiperiodically driven system. The analysis here is similar to that in Figure 1, but for traffic flow data collected by 47 detectors along the 408 highway of Florida state.

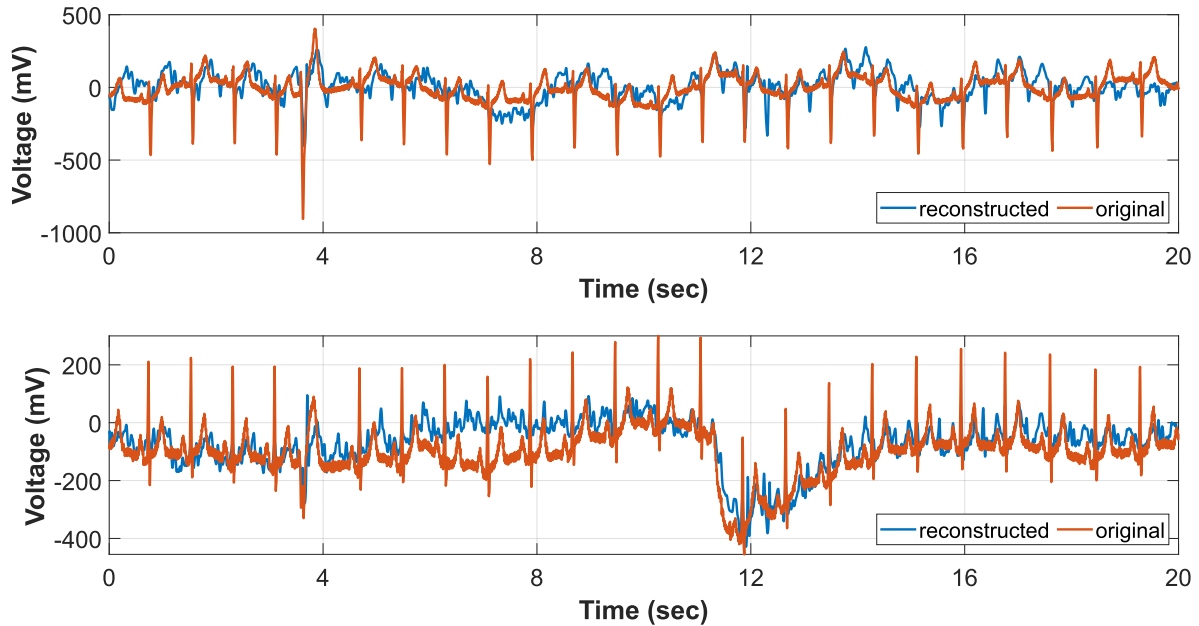


Figure 3: Human cardiac system as a quasiperiodically driven system. The analysis here is similar to that in Figure 1, but for atrial fibrillation (top) and atrial flutter (bottom) data obtained from patients. Unlike the traffic systems in the previous two examples, the heart has a non-smooth dynamics, driven by periodic but sudden firing of neurons. We selected this example as a test for the limits of our learning algorithm. The reconstruction error is higher, but correctly captures the periodicities and spiking events.

This completes the description of our problem. Assumptions 1, 2 and 3 will be the premise of our methods, and the task is to find or reconstruct the functions in (4). There are many challenges to accomplishing this task. We show in Section 2 that a dynamical system either has only one eigenfrequency ($=0$), or infinitely many. Moreover, if $d > 1$ in (1), then the eigenfrequencies are dense on the real line. This makes the task of separating these frequencies very challenging from a numerical point of view. Unlike DMD based or Fourier analysis based methods, we aim to obtain guarantees of convergence to the true discrete spectrum of the system. We discuss this in more detail in Section 4. Secondly, the task of finding the functions g_{per} and g_{chaos} cannot be carried out exactly. This is a classic learning / interpolation problem, and a blind machine-learning based approach could lead to widely divergent trajectories due to the chaotic nature of traffic dynamics. One of our innovations is the structure we propose in (4). See Table 2 for a comparison of our methods with other techniques, particularly DMD-based techniques.

Outline. A key consideration for us is *quasiperiodicity*. In Section 2 we discuss what it means, and also interpret the significance of the θ coordinates. A key component of our method is the use of kernel integral operators and the theory of reproducing kernel Hilbert spaces. We discuss these concepts and the relevant techniques in Section 3. The actual data-driven implementation of the theory is described in Section 4, where we operate under Assumption 3. Finally we use these techniques to analyze three real-world systems in Section 5.

2 Koopman operator and its spectrum.

The Koopman operator U converts the original nonlinear dynamics on a finite dimensional phase-space into a linear dynamics on an infinite dimensional vector space. It is a time-shift operator, operating on functions instead of points on the phase space. Given any function $\phi : \Omega \rightarrow \mathbb{R}$, $U\phi$ is another function defined as

$$(U\phi)(z) := \phi(Fz), \quad \forall z \in \Omega, \quad (5)$$

where F is the underlying dynamical system (1). ϕ can be interpreted as a measurement or observation on the phase space Ω , and $U\phi$ is the evolution / transformation of this measurement with the dynamics. Note that by virtue of (5) the correspondence $\phi \mapsto U\phi$ is linear. Thus the Koopman operator converts any nonlinear dynamical system into a linear map. This allows various tools from operator theory / functional analysis to be brought into the study of dynamics. The properties of U depends on the choice of vector/function space. Some common choices of function spaces are $C(\Omega)$ the space of continuous functions, or $C^r(\Omega)$, the space of r -times differentiable functions on Ω . We shall use the Hilbert space $L^2(\mu)$, the space of square-integrable functions with respect to an invariant measure μ of the dynamics. In this space, the Koopman operator is a unitary operator, a property which makes its spectrum have some desirable properties and be numerically accessible [19, 16, 20].

Koopman eigenfrequencies. Eigenvalue and eigenfunction pairs are one of the first attributes of an operator that are studied. For U , these carry a lot of significance. Since U is unitary, its spectrum must lie on the unit circle of the complex plane. The eigenvalues of U correspond to the point spectrum, and any eigenfunction ζ has a corresponding eigenvalue of the form $e^{i\omega}$ for some $\omega \in \mathbb{R}$. ω is called the Koopman eigenfrequency corresponding to ζ . We thus have

$$(U^n \zeta)(z) \stackrel{\text{by def.}}{=} \zeta(F^n z) = e^{i\omega n} \zeta(z), \quad \forall n \in \mathbb{N}. \quad (6)$$

Equation 6 reveals that the time-evolution of Koopman eigenfunctions is highly tractable, it is equivalent to multiplication by $e^{i\omega n}$ as a function of time n . Since $e^{i\omega}$ lies on the unit circle, its magnitude does not change and this also allows for stable prediction of the eigenfunction ζ . U always has the constant functions

as eigenfunctions with eigenfrequency 0. In general U may or may not have other eigenfrequencies. For the special structure (1) that we assume, the eigenfunctions of the driving system $\eta \mapsto \theta + \rho$ provides eigenfunctions for the dynamics under F . Suppose ζ is a Koopman mode for the driving system. Then we have :

$$\zeta(\theta_{n+k}) = e^{i\omega k} \zeta(\theta_n), \quad \forall k, n \in \mathbb{N}.$$

Then define $\bar{\zeta}(x, \theta) := \zeta(\theta)$. Then note that

$$\bar{\zeta}(x_{n+k}, \theta_{n+k}) = \zeta(\theta_{n+k}) = e^{i\omega k} \zeta(\theta_n) = e^{i\omega k} \bar{\zeta}(x_n, \theta_n), \quad \forall k, n \in \mathbb{N}.$$

Thus every eigenfunction for the driving system also leads to an eigenfunction for the entire system. If the driven system is chaotic, then this correspondence is one-to-one. We can now give a precise definition of the integer d in (1), in terms of *generating frequencies*.

Generating frequencies. The collection of eigenfunctions and (eigen)-frequencies have an algebraic structure to them. For any two frequencies ω_1, ω_2 , and integers a, b , $a\omega_1 + b\omega_2$ is also a frequency. This is because if z_1, z_2 are their corresponding eigenfunctions, then

$$z_1(\Phi^t x) = e^{i\omega_1 t} z_1(x), \quad z_2(\Phi^t x) = e^{i\omega_2 t} z_2(x).$$

As a result

$$(z_1^a z_2^b)(\Phi^t x) = z_1^a(\Phi^t x) z_2^b(\Phi^t x) = e^{i(a\omega_1 + b\omega_2)t} (z_1^a z_2^b)(x).$$

Thus integer linear combinations of frequencies are again frequencies, and products of eigenfunctions are again eigenfunctions. In particular, if the system has at least one nonzero frequency, then it has all harmonics of that frequency and thus infinitely many frequencies. A collection of eigenfrequencies are said to be independent if no integer linear combination of them is an integer. If the system has two independent frequencies, then all its frequencies are together dense on the real line. A collection of frequencies will be called a *basis* or *generating* set of eigenfrequencies if they are independent and all frequencies of the system can be generated by taking integer linear combinations of frequencies from this set. There is no unique choice of a basis, but all bases will have the same dimension d , called the quasiperiodicity dimension d . This number d is finite if Ω is a finite-dimensional manifold.

Koopman eigenfunctions as phase. An important realization for us is that we may assume without loss of generality that $|\zeta| \equiv 1$. This is because, under the additional assumption of ergodicity [see 19] we can assume that ζ is non-zero almost everywhere. Then if we set

$$\tilde{\zeta}(z) := \frac{\zeta(z)}{|\zeta(z)|},$$

it can be easily verified that $\tilde{\zeta}$ is also a Koopman eigenfunction with same frequency. Thus a Koopman eigenfunction can be interpreted as a phase, i.e., as a map

$$\zeta : \Omega \rightarrow S^1,$$

S^1 being the unit circle in the complex plane \mathbb{C} . According to (6), this phase rotates uniformly with speed ω . Koopman eigenfunctions thus reveal the intrinsic rotational / (quasi)-periodic factors embedded in chaotic dynamics. This quasiperiodic component may not be distinguishable from the phase space equations or from the measurements, but they affect the outcome of various numerical procedures carried on data produced by such systems [e.g. 19, 1, 21].

This interpretation of eigenfunctions as phase helps reveal torus dynamics embedded within the system.

Suppose we have a Koopman mode $\zeta : \Omega \rightarrow \mathbb{C}$ with eigenfrequency ω . Then by (6)

$$\zeta(F^n x) = e^{i\omega n} \zeta(x).$$

We had discussed before that we can assume without loss of generality that $|\zeta| \equiv 1$. Therefore the values of ζ trace out the unit circle on the complex plane. This leads to the factored dynamics :

$$\begin{array}{ccc} \Omega & \xrightarrow{F} & \Omega \\ \downarrow \zeta & & \downarrow \zeta \\ S^1 & \xrightarrow{R_\omega} & S^1 \end{array}$$

where R_ω is the uniform rotation by angular speed ω on the unit circle. Thus the original dynamics contains the circle rotation. In fact, if we take k Koopman eigenmodes simultaneously, we get rotation on a k -dimensional torus.

$$\begin{array}{ccc} \Omega & \xrightarrow{F} & \Omega \\ \downarrow \zeta_1, \dots, \zeta_k & & \downarrow \zeta_1, \dots, \zeta_k \\ \mathbb{T}^k & \xrightarrow{R_{\vec{\omega}}} & \mathbb{T}^k \end{array} \quad (7)$$

If these eigenfrequencies are independent, then this map will be surjective. Taking $d = k$ implies that the dynamics has an embedded / factor torus rotation, of the same dimension as the quasiperiodicity dimension.

Reconstructing quasiperiodicity. We now have the theoretical tools to describe our method to separate the coordinates of \mathbb{T}^d from Ω . Using results from Lie group theory [22, Thm 6], it can be shown that if a generating set of Koopman eigenfunctions are smooth, then the factor map in (7) becomes a submersion of manifolds, with constant fibre. This fibre can be interpreted as the manifold \mathcal{M} . It is unknown whether this factorization holds in an ergodic sense for the more general case of $L^2(\mu)$ eigenfunctions. If that is true then all the eigenfunctions of F would restrict to Fourier functions on the \mathbb{T}^d components. We proceed with this assumption and use Koopman eigenfunctions of F to discover the rotation dynamics on \mathbb{T}^d . The dimension d is an algebraic property of the set of Koopman eigenfunctions, and is defined through generating sets. We show in Section 4 how one can avoid the task of finding such a generating set, the quasiperiodicity dimension d , as well as rotation vector ρ , and still obtain a data-driven reconstruction.

This completes our examination of the quasiperiodic structure of the dynamics (1). We next discuss some techniques from Functional Analysis for reconstructing the quasiperiodic component and its complement.

3 Kernels and integral operators.

A kernel is a function $k : M \times M \rightarrow \mathbb{R}$ on some space M . The quantity $k(x, y)$ is measure of similarity, closeness or distance between two points $x, y \in M$. Kernel-based methods have been used very effectively to obtain geometric information of the underlying space M . This information has been used to study various related structures such as statistical manifolds [23], geometric information [24, 25, 26], and dynamical information such as tracer flows [10], Lyapunov functions [27], stable/unstable foliations [28], Koopman spectrum [29, 19, 16] and more generally the spectral measure [20]. The techniques in this paper are based on [16]. We shall use the *Gaussian kernel*

$$\kappa_\epsilon(x, y) := \exp\left(-\frac{1}{\epsilon} d(x, y)^2\right),$$

where ϵ is called the *bandwidth parameter*, and $d(\cdot, \cdot)$ is some notion of metric or distance on the space. Note that $\kappa_\epsilon(x, y) = 1$ iff $x = y$. It decays exponentially from 1 as y moves away from x . If ϵ is decreased, then

the function decays more sharply. For our purposes, $M = \Omega$, the phase-space of the dynamics. However, since we are working under the data-driven assumption 3, Ω will be assumed to be unknown and we need an indirect access to Ω . This is done through an embedding described below.

Delay-coordinates. The data sequence described in Assumption 3 is obtained through an observation Y . However Y may not faithfully replicate Ω , i.e., Y may not be a one-to-one map and its values may not correspond to unique states in Ω . An easy solution to this problem is the method of delay coordinates [e.g. 30, 31, 32], in which the dynamics is embedded in higher dimensional space $\mathbb{R}^{k(Q+1)}$, where Q is called the number of delays. The delay coordinated version of the map Y is the map

$$Y^{(Q)} : \Omega \rightarrow \mathbb{R}^{k(Q+1)}, \quad Y^{(Q)}(\omega) := (Y(\omega), Y(F^1\omega), \dots, Y(F^Q\omega)).$$

Thus the delay coordinated version of each point y_n is

$$y_n \leftrightarrow y_N^{(Q)} := (y_n, y_{n+1}, \dots, y_{n+Q}).$$

The main point of using delay coordinates, as explained in [30], is that for a typical observation map Y , if Q is large enough, then $Y^{(Q)} : \Omega \rightarrow \mathbb{R}^{k(Q+1)}$ is an embedding / one-to-one map. There are several heuristic algorithms to determine a Q which would be sufficiently large [e.g. 33, 34, 35, 36]. We proceed with the assumption that the Q chosen is large enough. We can then use the Gaussian shape function to implicitly obtain a kernel $k_\epsilon : \Omega \times \Omega \rightarrow \mathbb{R}$ as follows

$$k_\epsilon(z, z') := \kappa_\epsilon(Y^{(Q)}(z), Y^{(Q)}(z')) = \exp\left(-\frac{1}{\epsilon} \|Y^{(Q)}(z) - Y^{(Q)}(z')\|^2\right). \quad (8)$$

Even if the two states z, z' are unknown, the left hand side in (8) can be computed since the right hand side only uses the observation map Y . When using the Gaussian kernel directly with finite data, one can run into problems of undersampling or non-uniform density. As a remedy, one performs a series of normalizations on the basic kernel, to adjust for these deficiencies.

Bistochastic kernels. These are normalized / modified versions of k_ϵ which retain the symmetry along with additional properties such as Markov property. First we define two functions

$$\deg_R(z) := \int k_\epsilon(z, z') d\mu(z'), \quad \deg_L(z') := \int \frac{k_\epsilon(z, z')}{\deg_R(z)} d\mu(z).$$

These are called the right and left degree functions respectively. Next define a kernel

$$\tilde{k}_\epsilon(z, z'') := \frac{k_\epsilon(z, z'')}{\deg_R(z) \deg_L(z'')^{1/2}},$$

and finally set

$$p_\epsilon(z, z') := \int \tilde{k}_\epsilon(z, z'') \tilde{k}_\epsilon(z'', z') d\mu(z'').$$

The kernel p_ϵ is symmetric and has stronger properties, revealed by considering its associated *integral operator*.

Kernel integral operators. Given a C^r kernel $\kappa : \Omega \times \Omega \rightarrow \mathbb{R}$, the associated integral operator \mathcal{K} operates on $L^2(\mu)$ functions $\phi : \Omega \rightarrow \mathbb{R}$ as

$$(\mathcal{K}\phi)(z) := \int_{\Omega} \kappa(z, z') \phi(z') d\mu(z'),$$

leading to a C^r function $\mathcal{K}\phi$. The integral operators corresponding to the kernels \tilde{k}_ϵ and p_ϵ are denoted as \tilde{K}_ϵ and P_ϵ respectively, defined similarly as

$$(\tilde{K}_\epsilon\phi)(z) := \int_{\Omega} \tilde{k}_\epsilon(z, z')\phi(z')d\mu(z'), \quad (P_\epsilon\phi)(z) := \int_{\Omega} p_\epsilon(z, z')\phi(z')d\mu(z').$$

The kernels \tilde{k}_ϵ and p_ϵ have been designed so that we have the relation

$$P_\epsilon = \tilde{K}_\epsilon \tilde{K}_\epsilon^*.$$

It is a well known fact from Analysis that P_ϵ is a *compact*, symmetric operator on $L^2(\mu)$ [e.g, 20]. Moreover P_ϵ has a complete basis of eigenfunctions

$$P_\epsilon\phi_j = \lambda_j\phi_j, \quad j = 1, 2, \dots,$$

where the indexing is done so that the λ_j s are in decreasing order. Due to the normalizations carried out, we have $\phi_1 \equiv 1_\Omega$, the constant function equal to 1 everywhere. Moreover, the eigenvalues satisfy $1 = \lambda_1 \geq \lambda_2 \geq \lambda_3 \geq \dots > 0$. Also importantly, the ϕ_j are an orthonormal basis, i.e.,

$$\langle \phi_i, \phi_j \rangle_{L^2(\mu)} := \int \phi_i^*(x)\phi_j(x)d\mu(x) = \delta_{i,j}.$$

All these properties of the λ_j and ϕ_j are useful for *kernel-based learning*, in which we recreate or extrapolate an unknown function from some samples, using these ϕ_j s as a basis.

Kernel based learning. Two of the main advantages of kernel based approaches is that while the ϕ_j can be approximated to any degree of accuracy by solving an eigenvalue equation of a data-driven matrix [see Algorithm 1]; and they can be easily extended from vectors to a continuous function over the entire data space $\mathbb{R}^{k(|Q|+1)}$ and thus on Ω . The ϕ_j s also happen to be left singular vectors of the asymmetric operator \tilde{K}_ϵ , with $\sqrt{\lambda_j}$ and γ_j being the associated singular values and right singular vectors. Thus for an arbitrary point $z \in \mathbb{R}^{k(|Q|+1)}$, we have

$$\phi_j(z) = \lambda_j^{-1} \int p_\epsilon(z, z')\phi_j(z')d\mu(z') = \lambda_j^{-1} \int \tilde{k}_\epsilon(z, z')\gamma_j(z')d\mu(z'). \quad (9)$$

In a data-driven setting, these integrals are replaced by matrix multiplications, see Algorithm 4 in Section 4 for a precise description. These ϕ_j form the basis for *learning* any function $f : \mathbb{R}^{k(Q+1)} \rightarrow \mathbb{R}^d$. It is done by first computing the components of f along the first ϕ_j

$$f_l := \langle \phi_l, f \rangle_{L^2(\mu)} = \int_{\mathbb{R}^{k(Q+1)}} \phi_l^*(z)f(z)d\mu(z),$$

and then reconstructing f as $f = \sum_l f_l \phi_l$. Then by (9) we have for every $x \in \mathbb{R}^{k(Q+1)}$,

$$f(x) = \sum_l f_l \phi_l(x) = \frac{1}{\deg_R(x)} \int k_\epsilon(x, y) \sum_l f_l \tilde{\gamma}_l(y) d\mu(y) = \frac{\langle k_x, w \rangle_{L^2(\mu)}}{\langle k_x, 1 \rangle_{L^2(\mu)}}, \quad w := \sum_l f_l \frac{1}{\lambda_l} \gamma_l,$$

where k_x is the function $k(x, \cdot)$, known as the *kernel section* at x . The function w is called the *feature vector* corresponding to the function f . The correspondence between f and w is linear and via an operator $Feature : L^2(\mu) \rightarrow L^2(\mu)$. The function $w = Feature(f)$ plays the role of a density function. The value of $f(x)$ then becomes the transition probability via the Markov transition function $k_\epsilon^{\text{Markov}}$, namely,

$$f(x) := \int k_\epsilon^{\text{Markov}}(x, y)w(y)d\mu(y).$$

In practice, instead of doing an infinite sum of the form \sum_l , we use

$$f(y) \approx \sum_{l=1}^L f_l \phi_l(y) = \int_{\mathbb{R}^{k(Q+1)}} p_\epsilon(y, z) \sum_{l=1}^L \frac{f_l}{\lambda_l} \phi_l(z) d\mu(z).$$

The parameter L is called the *spectral truncation* parameter. The higher the value of L , the more accurate the approximation is. However, from a practical point of view, higher order eigenfunctions / eigenvectors are more difficult to be computed, and carry more computational error. The division by λ_l , which goes to zero as $l \rightarrow \infty$ also restricts how big L could be, for a given computational resources and data-size.

This completes a description of the theoretical basis of our methods. We next discuss the procedure in the data-driven setting of Assumption 3. There, we also discuss the procedure for frequency identification in Algorithm 2.

4 The data-driven procedure.

In a data-driven approach, all of the spaces, operators and maps described in Section 3 are approximated via data. This begins with an approximation of the dynamics-invariant measure μ by the *sampling measure*

$$\mu_N = \frac{1}{N} \sum_{n=1}^N \delta_{y_n^{(Q)}},$$

the average of the Dirac-delta measure on the data points $y_n^{(Q)}$. These approximate μ in a weak-sense via their integrals for every continuous test function $\phi : \mathbb{R}^{k(Q+1)} \rightarrow \mathbb{R}$:

$$\int_{\mathbb{R}^{k(Q+1)}} \phi d\mu_N = \frac{1}{N} \sum_{n=1}^N \phi(y_n^{(Q)}) \xrightarrow{n \rightarrow \infty} \int_{\mathbb{R}^{k(Q+1)}} \phi d\mu.$$

As a result, the infinite dimensional Hilbert space $L^2(\mu)$ will be represented as $L^2(\mu_N)$. The kernel integral operators K , \tilde{K} and P will be represented by $N \times N$ matrix $[K]$, $[\tilde{K}]$ and $[P]$, as described below :

Algorithm 1 (Kernel building).

1. *Input :*

- (i) Data $\{y_n \in \mathbb{R}^k : n = 1, \dots, N\}$ as in Assumption 3.
- (ii) Bandwidth parameter $\epsilon > 0$ for the kernel.
- (iii) The number of eigenvectors $L \in \mathbb{N}$ to be computed.
- (iv) Number of delay-coordinates Q .

2. *Output*

- (i) Eigenfunctions $\{\vec{\phi}_l : l = 1, \dots, L\}$ and eigenvalues $1 = \lambda_1 \geq \dots \geq \lambda_L$ of a bistochastic, symmetric kernel $p_\epsilon(x, y)$.
- (ii) Right singular vectors $\{\vec{\gamma}_l : l = 1, \dots, L\}$.

3. *Steps*

- (i) Compute a $N \times N$ kernel matrix $[K]$ using the Gaussian kernel k_ϵ (8) as :

$$[K]_{i,j} := k_\epsilon(y_i^{(Q)}, y_j^{(Q)}), \quad 1 \leq i, j \leq N.$$

(ii) Compute the degree vectors

$$\vec{d} := \frac{1}{N} [K] \vec{1}_N, \quad D := \text{diag}(\vec{d}), \quad \vec{q} := \frac{1}{N} [K] D^{-1},$$

and then the matrix

$$[\tilde{K}] := D^{-1} [K] Q^{-0.5}, \quad Q := \text{diag}(\vec{q}).$$

(iii) Compute the top L singular values $1 = \sigma_1 \geq \dots \geq \sigma_L$ of $[\tilde{K}]$ and the corresponding left eigenvectors $\vec{\phi}_1, \dots, \vec{\phi}_L$ and right singular vectors $\vec{\gamma}_1, \dots, \vec{\gamma}_L$.

(iv) Set $\lambda_i := \sigma_i^2$, for $i = 1, \dots, L$.

Algorithm 1 is an initial processing step on the data. It is not specific to the reconstruction problem for the dynamics. The role of the bandwidth ϵ in numerical experiments is discussed in Section 5. The output of the algorithm can be used for any learning problem based on the given dataset. The set of vectors $\{\vec{\phi}_l : l = 1, \dots, L\}$ and $\{\vec{\gamma}_l : l = 1, \dots, L\}$ are both orthonormal systems for \mathbb{C}^N . The N -dimensional vectors $\vec{\phi}_l$ have continuous extensions to the whole of $\mathbb{R}^{k(Q+1)}$ as

$$\bar{\phi}_l : \mathbb{R}^{k(Q+1)} \rightarrow \mathbb{R}, \quad \bar{\phi}_l(y) := \frac{1}{N\lambda_l} \vec{k}_\epsilon(y)^\top \vec{\gamma}_l, \quad \vec{k}_\epsilon(y) := \left(\tilde{k}_\epsilon(y, y_1^{(Q)}), \dots, \tilde{k}_\epsilon(y, y_N^{(Q)}) \right). \quad (10)$$

The function $\bar{\phi}_l$ is as smooth as the kernel k_ϵ . If y in the above equation is substituted by one of the data-points $y_n^{(Q)}$, then by design

$$\bar{\phi}_l(y_n^{(Q)}) = \vec{\phi}_{l,n}.$$

Thus $\bar{\phi}_l$ is indeed a continuous extension of the vector $\vec{\phi}_l$. This feature of extendability and easy evaluation at arbitrary points is one of the most powerful tools of kernel-based methods. In our next algorithm, we show a different application of these eigenfunctions, for discovering true Koopman eigenfrequencies. It is based on ergodic theoretic results derived in [16]. It involves using the familiar fast-Fourier transform, but on the L eigenfunctions derived above instead of the raw data, along with a weighting using the λ_l s. The results are interpreted in a functional space called a *reproducing kernel Hilbert space* or RKHS.

Algorithm 2 (RKHS based spectral analysis). [16, Alg. 1].

1. Input

(i) Eigenfunctions $\{\vec{\phi}_l : l = 1, \dots, L\}$ and eigenvalues $1 = \lambda_1 \geq \dots \geq \lambda_L$ from Algorithm 1.

(ii) Threshold parameters : $\epsilon_1, \epsilon_2 > 0$ and integer L_0 such that $1 < L_0 < L$.

(iii) Sampling interval Δt if the source is a continuous time system.

2. Output : A set of frequencies identified $0 = \omega_1 < \omega_2 < \dots < \omega_m$ identified as true Koopman eigenfrequencies.

3. Steps

(i) Collect the eigenvectors $\vec{\phi}_l$ in an $N \times L$ matrix $[\Phi]$. Let \mathcal{F}_N be the discrete Fourier transform on N vectos. Set $\Lambda := \text{diag}(\lambda_1, \dots, \lambda_L)$ and compute

$$[\hat{\Phi}] := \mathcal{F}_N [\Phi] \quad [H] := [\hat{\Phi}] \Lambda^{-0.5}.$$

(ii) Next compute an $N \times L$ matrix $[W]$ such that for each $n = 1, \dots, N$,

$$[W]_{n,1} := |[H]_{n,1}|, \quad [W]_{n,l+1} := [W]_{n,l} + |[H]_{n,l+1}|, \quad l = 1, \dots, L-1.$$

- (iii) Set $J = 1, \dots, N$.
- (iv) Discard all the $j \in J$ for which $[W]_{j,L_0} < \epsilon_1$.
- (v) Of the remaining $j \in J$, discard those j for which $\ln[W]_{j,L} - \ln[W]_{j,L_0} > \epsilon_2$.
- (vi) Compute $\omega_j = \frac{2\pi j}{N}$ for all of the remaining $j \in J$.
- (vii) If the underlying system is continuous time, then divide each of the ω_j by Δt .

Note that there are two filterings taking place, in steps (iii) and (iv), via parameters ϵ_1 and ϵ_2 respectively. They are based on results in approximation theory on Reproducing kernel Hilbert spaces [see 16, Thm 1, 4]. The identified frequencies $0 = \omega_1 < \omega_2 < \dots < \omega_m$ are by no means exhaustive, they are only a finite subset of an usually infinite set of Koopman eigenfrequencies. However, they represent those (true) frequencies which have a significant presence in the data. The threshold ϵ_1 is meant to be a numerical implementation of frequencies being significant. We shall use these selected frequencies later to build our reconstructed dynamics (4). Algorithm 2 is unique in its use of RKHS-regularity as a criterion for identifying frequencies. See Table 2 for a comparison of our methods with other techniques.

We utilize the delay-coordinate structure in the embedding to simplify the construction of $g_{chaos} : \mathbb{R}^{k(Q+1)} \rightarrow \mathbb{R}^k$ as

$$g_{chaos}(x^{(0)}, \dots, x^{(Q)}) := \begin{bmatrix} g_{chaos}^{(0)}(x^{(0)}, \dots, x^{(Q)}) \\ x^{(0)} \\ \vdots \\ x^{(Q-1)} \end{bmatrix} \quad (11)$$

Here for each $q \in 0, \dots, Q$, $x^{(q)}$ is the q -th set of coordinates in \mathbb{R}^k . We next describe reconstruct the periodic and chaotic components g_{per} and $g_{chaos}^{(0)}$. The set of Koopman eigenfrequencies identified from Algorithm 2 can be passed as the second input to the Algorithm below. Given a matrix $[E]$, we use $[E]_{l,:}$ to denote its l -th row. Also recall the functions $\bar{\phi}_l$ defined in (10).

Algorithm 3 (Components of the dynamics).

1. *Input*

- (i) An $N \times k$ matrix $[Y]$ whose n -th row represents the data point $y_n \in \mathbb{R}^k$ as in Assumption 3.
- (ii) A set of Koopman eigenfrequencies $0 = \omega_1 < \omega_2 < \dots < \omega_m$.
- (iii) $N \times L$ matrix Φ whose columns store the eigenfunctions $\bar{\phi}_l$ from Algorithm 1.

2. *Output :*

- (i) $L \times k$ matrix $[E]$ which approximates the function

$$g_{chaos}^{(0)} : \mathbb{R}^{k(Q+1)} \rightarrow \mathbb{R}^k, \quad g_{chaos}^{(0)} \approx \sum_{l=1}^L [E]_{l,:} \bar{\phi}_l. \quad (12)$$

- (ii) $m \times k$ matrix $[A]$ which represents a periodic function

$$g_{per} : \mathbb{R} \rightarrow \mathbb{R}^k, \quad g_{per}(t) := \Re \sum_{j=1}^m [A]_{j,:} e^{i\omega_j t}. \quad (13)$$

3. *Steps*

- (i) Define an $N \times m$ matrix $[F]$ as

$$[F]_{n,j} := (2 - \delta_{j,1}) e^{i n \omega_j} \quad 1 \leq n \leq N, 1 \leq j \leq m.$$

(ii) Find an $m \times k$ matrix A which is the least-squares solution to

$$\Re[F][A] = [Y]$$

(iii) Set $[Y_{non}] := [Y] - \Re[F][A]$ and the $L \times k$ matrix $[E] := [\Phi]^* [Y_{non}]$.

Algorithms 1, 2 and 3 reconstructs the quasiperiodically driven dynamics which underlies the data. We shall describe another algorithm to perform the evaluations of the functions $\bar{\phi}_l$ as in (12).

Algorithm 4 (Out of sample evaluations).

1. *Input*

(i) Data $\{y_n \in \mathbb{R}^k : n = 1, \dots, N\}$ as in Assumption 3, along with sampling interval Δt if the source is a continuous time system.

(ii) $L \times k$ matrix $[E]$ from Algorithm 3.

(iii) Vector $y \in \mathbb{R}^{k(Q+1)}$ representing a point of evaluation.

2. *Output* : vector $g_{chaos}^{(0)}(y) \in \mathbb{R}^k$.

3. *Steps*

(i) Create an $N \times L$ matrix $[\tilde{\Gamma}]$ defined as $[\tilde{\Gamma}]_{n,l} := \Gamma_{n,l} \lambda_l^{-1/2} \tilde{q}_n^{-1}$.

(ii) Next compute

$$\vec{k}_{os} := \left(k_\epsilon \left(y_n^{(Q)}, y \right) \right)_{n=1}^N, \quad s := \frac{1}{N} \sum_{n=1}^N k_{os}(n).$$

(iii) Finally compute

$$(e_1(y), \dots, e_k(y)) \approx \frac{1}{N_s} \vec{k}_{os}^\top [\tilde{\Gamma}][E].$$

The reconstruction. The m eigenfrequencies identified by Algorithm 2 are generated by some collection of d eigenfrequencies $\vec{\omega} = \tilde{\omega}_1, \dots, \tilde{\omega}_d$. Each selected frequency ω is thus of the form $\omega = \vec{j} \cdot \vec{\omega}$ for some d -dimensional integer vector $\vec{j} = (j_1, \dots, j_d)$. Then the periodic part g_{per} can be written as the Fourier series

$$g_{per}(\vec{\theta}) = \sum_{\vec{j} \in \mathbb{Z}^d} a_{\vec{j}} \exp(\iota(\vec{j} \star \vec{\omega}) \cdot \vec{\theta}),$$

where $\vec{j} \star \vec{\omega}$ is the d -dimensional vector $(j_1 \tilde{\omega}_1, \dots, j_d \tilde{\omega}_d)$. The output of Algorithm 2 provides a means of avoiding the task of identifying $\vec{\omega}$. The ω that are selected correspond to those indices \vec{j} for which $|a_{\vec{j}}|$ is substantial. Thus we have the approximation

$$g_{per}(\vec{\theta} + n\vec{\omega}) \approx \sum_{j=1}^m a_j \exp(\iota n \omega_j), \quad n = 0, 1, 2, \dots \quad (14)$$

Using this simplification 14, and the formulas in (12) and (13), we create the following data-driven model of the dynamics :

$$\boxed{\begin{aligned} y_{n+1}^0 &:= g_{per}(n\Delta t) + g_{chaos}^{(0)}(y_n^0, \dots, y_n^Q) \\ y_{n+1}^1 &:= y_n^0 \\ &\vdots \\ y_{n+1}^Q &:= y_n^{Q-1} \end{aligned}}, \quad y_n^q \in \mathbb{R}^k, \quad q \in 0, \dots, Q, \quad n = 1, 2, 3, \dots \quad (15)$$

Table 1: Summary of parameters in experiments. In all these experiments, $N = 2 \times 10^4$ and $\epsilon_1 = 0.1$.

Data-source	Figures	ϵ	Q	L_0	ϵ_2
CFX408	2, 5, 7	0.3	50	100	3.1
Signalized intersections	1, 4, 6,	0.1	50	100	4.0
Heart atrial data	3	0.002	50	500	5.1

This completes the statement of our methods and theory. We next show that the hypothesis of quasiperiodically driven dynamics proves effective for analyzing data from several real-world systems.

5 Case studies.

We analyze data from three real-world systems using our techniques from the previous sections.

1. Traffic dynamics on highway. Traffic flow is a critical parameter to understand highway traffic dynamics. Traffic flow refers to the number of vehicles passing through any cross section of a road. We obtained highway traffic flow data from US 408 which is a tolled expressway situated in Orlando, Florida, United States. We used proprietary traffic flow data collected from 64 sensors placed along a 22-mile corridor. We used the dataset provided by [Central Florida Expressway Authority \(CFX\)](#) in which outliers and faulty detectors were corrected. See Figure 2 for a view of the data, and its reconstruction, and Figure 5 for a more magnified view.
2. Traffic dynamics along signalized intersections. Queue length i.e. the number of stopped vehicles at an intersection during red lights is a indicator of the dynamics in an urban area. In this study we obtained queue length data from 9 signalized intersections of the Alafaya Corridor of Orlando city. This proprietary dataset was provided by [InSync](#) and first used in [37]. The dataset contains the queue lengths aggregated over every 2 min which is the approximate traffic-signal cycle duration. See Figure 1 for a view of the data, and its reconstruction, and Figure 4 for a more magnified view.
3. Cardiac signals. The data was obtained from [PhysioNet](#)'s repository of medical data. The data was collected in a study on the use of R-R intervals for detecting atrial fibrillation [38]. The data is a timeseries covering a time duration of 2 hours, sampled at 250 samples per second. The timeseries contained two columns representing unedited recordings of atrial fibrillation and atrial flutter, with 12-bit resolution over a range of ± 10 millivolts.

Our numerical methods has three main objectives

- (i) Reconstruction : Figures 5 and 4 provide a zoomed view of the reconstruction plots. They reveal the same level of accuracy over smaller time-scales of a day instead of weeks. Given a reference timeseries y_n , and a reconstruction \hat{y}_n , the *amplitude normalized, moving averaged error* is

$$e_{T,n} := \frac{1}{\|y\|_{\sup}} \frac{1}{T} \sum_{t=0}^{T-1} [\hat{y}_{n+t} - y_{n+t}], \quad n = 0, 1, 2, \dots \quad (16)$$

See Figure 10 for the calculation of these errors, and the rationale behind this choice. The magnitude of this error is about 15%, 0.7% and 3% respectively for the CFX408, Alafaya and Cardiac data experiment.

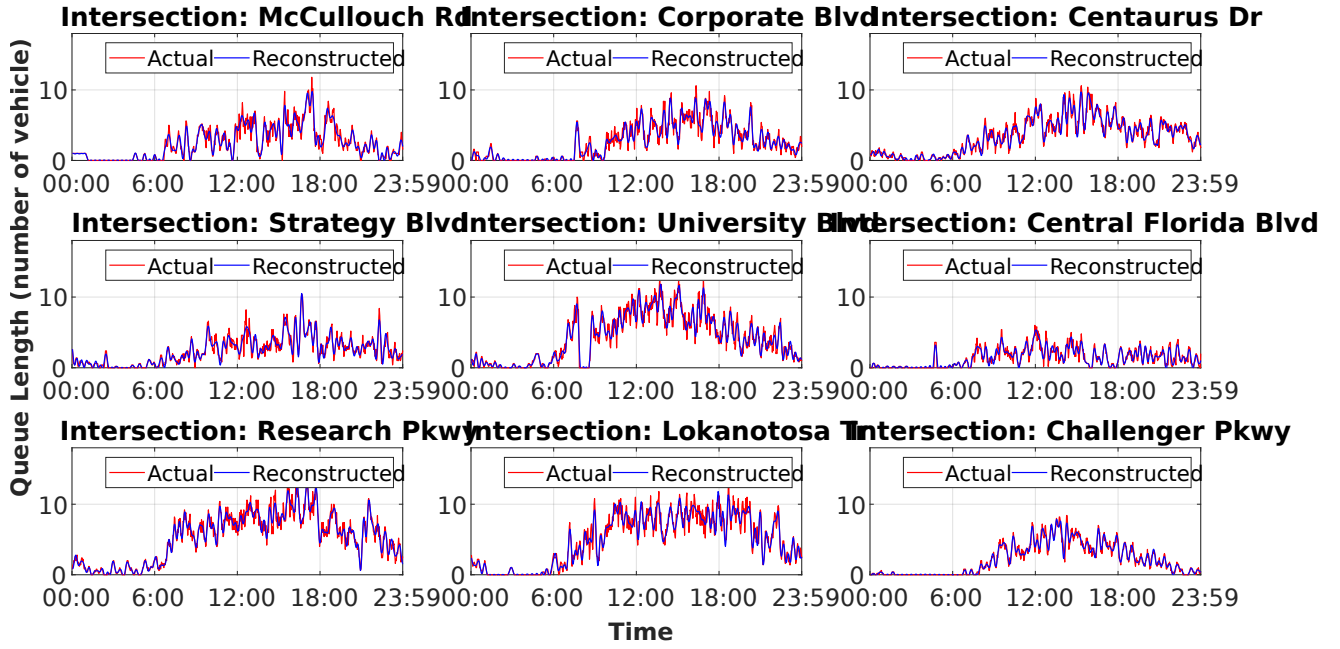


Figure 4: Closer look at the reconstruction of traffic queue-length dynamics. The results shown in Figure 1 is examined on a smaller time-scale of a day. The reconstruction appears accurate and coherent with the original traffic data.

- (ii) Identifying frequencies : Natural frequencies of the system contribute to the basic understanding of dynamical systems. They reveal the timescales as well as the quasiperiodicity dimension. These are displayed in Figure 8.
- (iii) Identifying coherent spatiotemporal modes : In systems such as traffic systems, one has a direct interpretation of some of the variables as spatial coordinates, which vary with time. Spatiotemporal patterns such as those in Figures 6, 6 represent components of the dynamics which is periodic in a combined space-time coordinate system.

We next discuss some important aspects of our numerical reconstruction, brought to light by these results.

Aliasing. Aliasing is a phenomenon created due to a discrete time sampling of any continuous time dynamical system. The effect of aliasing is not increased or decreased by the choice of method for analyzing the spectrum. It's effect is seen unavoidably in any numerical analysis of the spectrum. Henceforth, we shall call Koopman eigenfrequencies or eigenvalues as just eigenfrequencies or eigenvalues.

Recall that an eigenfrequency of ω of the continuous time dynamical system (or flow) $\{\Phi^t : M \rightarrow M : t \in \mathbb{R}\}$ results in the eigenvalue $e^{t\Delta\omega}$ for the discrete time analog $\Phi^{\Delta t} : M \rightarrow M$. The problem arises due to the 2π -periodicity of the function $x \mapsto e^{ix}$. The infinite real line \mathbb{R} is stretched by $1/\Delta t$ and wrapped around the circle represented by $[0, 2\pi]$. As a result, if there were two eigenfrequencies of the continuous time system ω', ω'' such that $\omega'' = \omega' + n2\pi/\Delta t$, both lead to the same eigenvalue :

$$e^{t\Delta t\omega'} = e^{t\Delta t\omega''} = \lambda.$$

If ζ' and ζ'' were eigenvectors corresponding to ω', ω'' , then note that

$$\zeta'(\Phi^{\Delta t}x) = \lambda\zeta'(x), \quad \zeta''(\Phi^{\Delta t}x) = \lambda\zeta''(x)$$

Conversely, if $\lambda = e^{t\omega}$ is an eigenvalue of the map $\Phi^{\Delta t}$, then it could correspond to any of the infinite set of

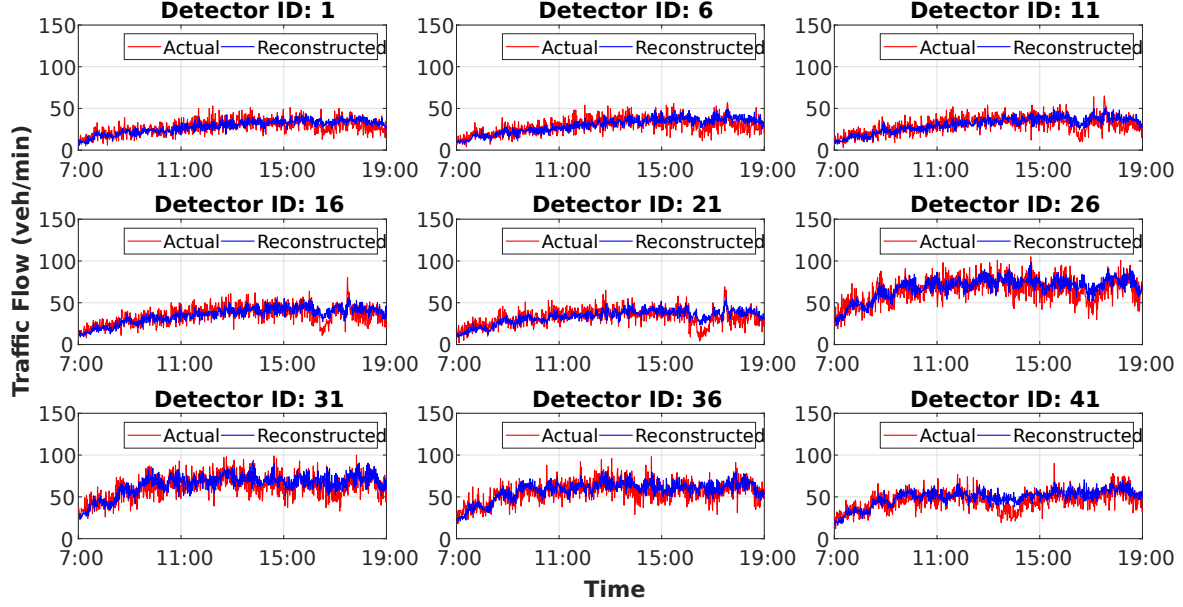


Figure 5: Closer look at the reconstruction of highway traffic flow data. The results shown in Figure 2 is examined on a smaller time-scale of a day. The reconstruction appears accurate and coherent with the original traffic data.

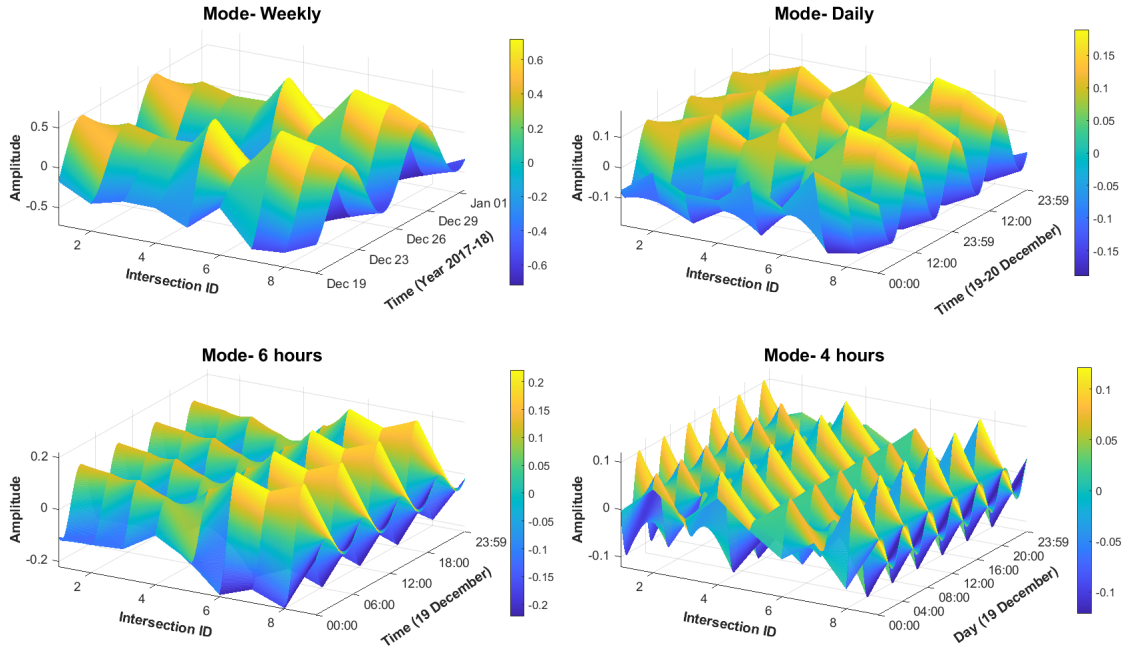


Figure 6: Koopman modes for traffic intersection dynamics. The traffic queue length build-up on the Alafaya highway is assumed to be driven by a quasiperiodically driven dynamics, of the form (4). The Koopman eigenmodes of this dynamics were extracted using purely data-driven means (Algorithms 1, 2). The describe coherent spatiotemporal patterns present within the dynamics.

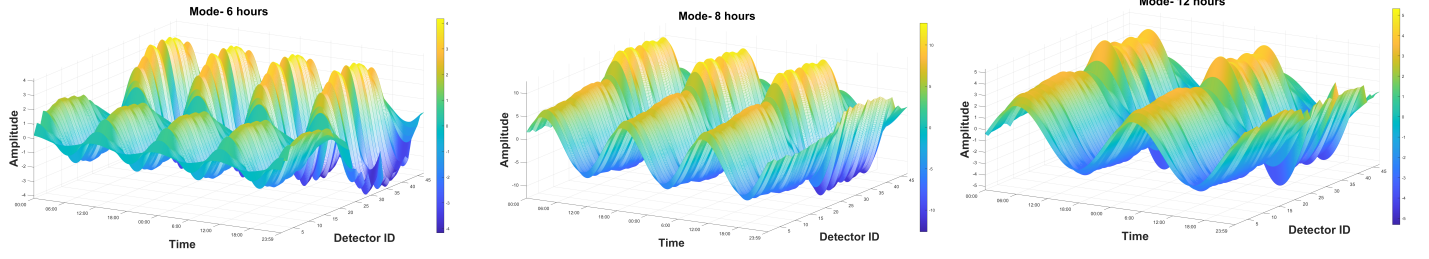


Figure 7: Koopman modes for highway traffic dynamics. The flux of traffic flow along the Florida 408 highway is assumed to be driven by a quasiperiodically driven dynamics, of the form (4). The Koopman eigenmodes of this dynamics were extracted using purely data-driven means (Algorithms 1, 2). The describe coherent spatiotemporal patterns present within the dynamics.

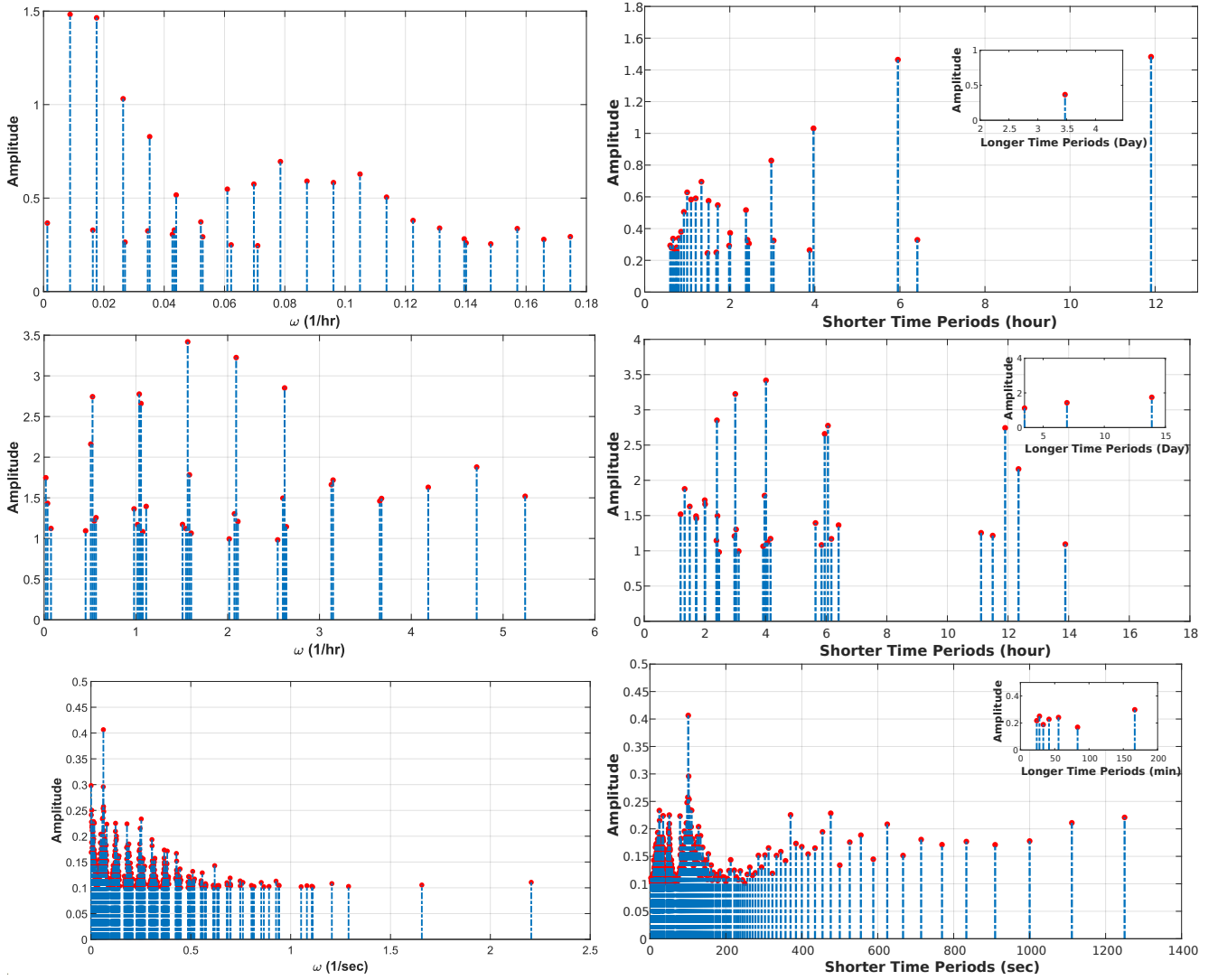


Figure 8: Selected frequencies and time-periods. The top, middle and bottom panels correspond to CFX408, Alafaya and the cardiac data respectively. The identified frequencies correspond to Koopman frequencies of the dynamical system (4) that we conceptually associate with the data. They can be interpreted as natural frequencies of these systems. Each time period T that is marked corresponds to a selected frequency ω via the relation $T = 2\pi/\omega\Delta T$, with ΔT being the sampling interval for the data.

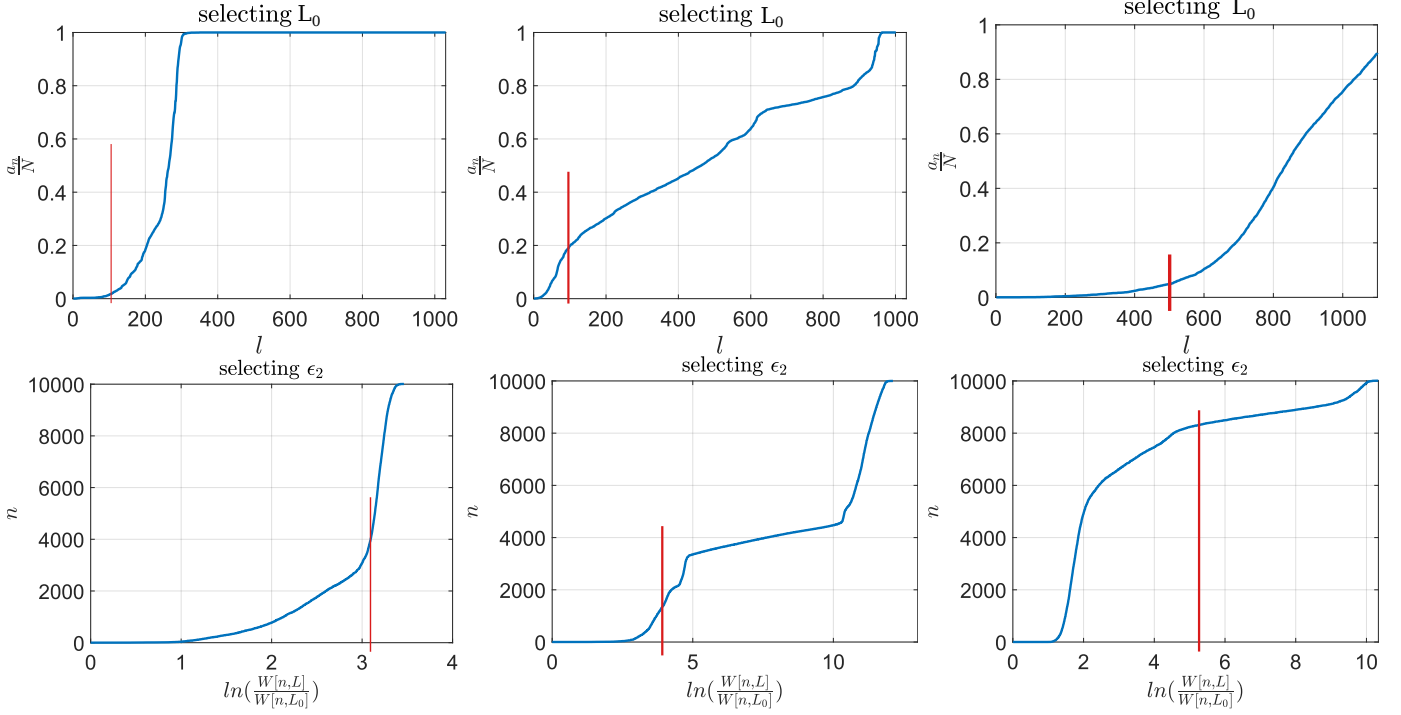


Figure 9: Choosing the thresholds L_0, ϵ_2 for the three experiments. The left panels correspond to CFX408, the middle panels to Alafaya, and the rightmost panels to the atrial fibrillation data. The red vertical lines correspond to major changes in the slop of the graph and indicate the choice of these parameters. The top panels correspond to the choice of L_0 , and the bottom panels to ϵ_2 . Lower the value of ϵ_2 , more frequencies get filtered out and higher the probability of the identification being correct. See Table 1 for a complete list of values for L_0, ϵ_2 as well as other parameters.

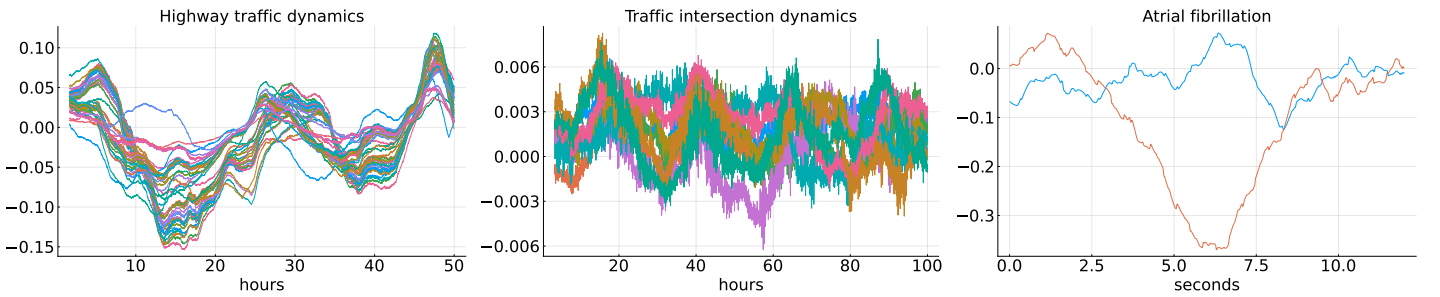


Figure 10: Error analysis for the reconstructed dynamics. The amplitude normalized moving average error (16) is computed for the three experiments, with a moving average window of 500 time units. The number of curves in each plot corresponds to k , the dimension of the signal used for analysis in that experiment. The use of a moving average window reduces the effect of random outliers or events. It diminishes the contribution of stochasticity to the error. Usually, when there is a mismatch between two dynamical systems such as the true dynamics (4) and the reconstruction (15), the two systems diverge and the error grows unrestricted. However, due to the special structure of quasiperiodically driven dynamics, and our ability to reconstruct the periodic part with high accuracy, our error does not grow monotonically but makes small oscillations.

frequencies $\{\omega + n\frac{2\pi}{\Delta t} : n = \dots, -2, -1, 0, 1, 2, \dots\}$. This ambiguity is the source of the problem of aliasing. The angular part ω of the eigenvalue λ is the only representative of an infinite number of translations of a single frequency. If one fixes a fundamental interval such as $[0, 2\pi/\Delta t]$ or equivalently $[-\frac{\pi}{\Delta t}, \frac{\pi}{\Delta t}]$, and if the flow Φ^t does not have any eigenfrequencies outside the fundamental interval, then there would not be any effect of aliasing. Thus however is never the case. Remedies to the effect of aliasing in a dynamical context would be

1. Using two different sampling frequencies, in a technique outlined in [16, Corr 2].
2. Passing the signal through a low pass filter that still preserves the dynamics information contained in the signal.

We are currently investigating ways to incorporate these techniques into our analysis. One effect of aliasing that is also visible in our calculations is known as *Nyström phenomenon*. It is seen as the presence of the frequency lowest non-zero $\frac{1}{N\Delta t}$ in our RKHS based analysis of the signal.

Choice of parameters. The numerical procedure has several parameters associated with it, as summarized in Table 1. For making the experiments more comparable, we chose the same size N for the data, and the parameter ϵ_1 . The bandwidth ϵ of the kernel and the number of delays Q need to be chosen suited to the data. A small ϵ captures more geometric information but could lead to a problem of undersampling. An $\epsilon \approx 0.01k$ seems to be a good choice for most cases. The number of delays Q is set using the correlation based method [36]. Figure 9 describes a heuristic procedure for selecting the parameters $L_0, \epsilon_1, \epsilon_2$. These three parameters filter the candidate frequencies based on two criterion - their strengths in the original signal as well as the RKHS regularity of their associated wave forms [see 16, Sec 8].

Learning non-smooth dynamics. Out of the three case studies, the reconstruction of the heart atrial data has the highest error, as seen in Figure 3. The electrical signals in the heart are intermittent, their spiking or firing behavior makes it a highly non-smooth system. Non-smooth systems pose a major challenge for learning problems. The authors are currently investigating an extension of the model in (4) that incorporates this spiking behavior structurally.

Conclusions. We have thus shown the following :

- (i) The use of two different thresholds ϵ_1 and ϵ_2 in our core Algorithm 2 is based on the asymptotic behavior in two different directions, provide a surer guarantee of identification of true eigenfrequencies and the discarding of *spurious* or *pseudo-spectrum* [e.g. 20, Sec 4.2].
- (ii) Applicability to chaotic dynamics : A unique aspect of our methods is that the methods are applicable to the analysis of signals in which the periodic component is either non-dominant or even absent. For such signals, both DMD-based techniques and Fourier techniques fails to identify the true eigenfrequencies.
- (iii) Smoothness of reconstruction : an inherent advantage of kernel-based techniques is the easy extrapolation from data to the entire data-space. Moreover, these interpolated functions have the same degree of smoothness as the kernel. The oscillatory behaviour of the kernel eigenfunctions increase with the index l and the choice of the spectral resolution parameter controls the smoothness of our interpolation.
- (iv) Out of sample evaluation : is essentially the task of extrapolation, i.e., evaluating functions reconstructed using the kernel, at points not in the original data-set. At each step of the iteration of (15), we perform these evaluations using Algorithm 4.

Table 2: Various techniques for identifying the natural / Koopman eigenfrequencies of dynamical systems, and their performance based on various parameters.

	Fourier averaging	EDMD	HDMD	Neural networks with memory	RKHS	Non-parametric regression
Related works	[39] [1]	[40] [41, 42, 43]	[44]	[45] [46], [47, 48, 49, 50]	[51, 52] [53, 16, 54]	[55, 56, 57, 58]
Avoids dense $N \times N$ matrix	Y	N	N	Y	Y	Y
Applicable to chaotic systems	N	N	N	N	Y	N
Applicable to systems with mixed spectrum	N	N	N	Y	Y	N
Explicit re-construction	Y	N	N	N	Y	Y
Higher accuracy for quasiperiodic systems	Y	Y	Y	N	Y	N
Low cost of iteration	Y	Y	Y	Y	N	N

- (v) Boundedness of reconstructed dynamics : A crucial advantage that kernel based methods offer over methods such as linear or polynomial regression, is that the interpolation is bounded, due the decaying nature of the kernel (8). All reconstructed dynamical models have some difference with the true system. This difference / defect is inevitable in a learning problem. If the reconstruction of g_{per} is bounded, then it would guarantee that the dynamics under (4) would remain bounded, and the deviation of the trajectories also remain bounded.

We have compared our kernel based method with other spectral estimation techniques in Table 2. One key aspect of using Gaussian kernels is that it leads to the creation of sparse $N \times N$ matrices, which lead to efficient computation and more economical memory usage. The out of sample reconstruction via (15) also given an explicit formula for the learnt / interpolated function. Another advantage our method derives from the theoretical results of [16] is that it can handle generated not only by periodic sources but by systems with purely chaotic or mixed spectrum.

References.

- [1] S. Das and J. Yorke. Super convergence of ergodic averages for quasiperiodic orbits. *Nonlinearity*, 31:391, 2018.

- [2] M Herman. Sur la conjugaison différentiable des difféomorphismes du cercle à des rotations. *Publications Mathématiques de l'Institut des Hautes Études Scientifiques*, 49:5–233, 1979.
- [3] M. Herman. *Mesure de Lebesgue et nombre de rotation*, volume 597. Springer, 1979.
- [4] V. Arnold. Small denominators. i. mapping of the circumference onto itself. *Amer. Math. Soc. Transl. (2)*, 46:213–284, 1965.
- [5] S. Das, Y. Saiki, E. Sander, and J. Yorke. Solving the Babylonian problem of quasiperiodic rotation rates. *Discrete Contin. Dyn. Syst.*, 12:2279–2305, 2019.
- [6] A. Avila and I. Mezić. Data-driven analysis and forecasting of highway traffic dynamics. *Nature Comm.*, 11(1):1–16, 2020.
- [7] E. Ling, L. Zheng, L. J Ratliff, and S. Coogan. Koopman operator applications in signalized traffic systems. *IEEE Trans. Intell. Transportation Sys.*, 2020.
- [8] R. Vautard and M. Ghil. Singular spectrum analysis in nonlinear dynamics, with applications to paleoclimatic time series. *Phys. D*, 35:395–424, 1989.
- [9] J. Slawinska and D. Giannakis. Spatiotemporal pattern extraction with data-driven Koopman operators for convectively coupled equatorial waves. In A. Banerjee, W. Ding, J. Dy, V. Lyubchich, and A. Rhines, editors, *Proceedings of the 6th International Workshop on Climate Informatics*, pages 49–52, Boulder, Colorado, 2016.
- [10] D. Giannakis and S. Das. Extraction and prediction of coherent patterns in incompressible flows through space-time Koopman analysis. *Phys. D*, 402:132211, 2019.
- [11] G. Froyland, S. Lloyd, and N. Santitissadeekorn. Coherent sets for nonautonomous dynamical systems. *Physica D*, 239(16):1527–1541, 2010.
- [12] G. Froyland, G. A. Gottwald, and A. Hammerlindl. A computational method to extract macroscopic variables and their dynamics in multiscale systems. *SIAM J. Appl. Dyn. Sys.*, 13(4):1816–1846, 2014.
- [13] G. Foster and A. Hubler. Optimal resonance forcing of nonlinear systems. *Bull Amer. Phys. Soc.*, 2006.
- [14] J. Zhu, R. Kuske, and T. Erneux. Tipping points near a delayed saddle node bifurcation with periodic forcing. *SIAM J. Appl. Dyn. Sys.*, 14(4):2030–2068, 2015.
- [15] S. Das and J. Yorke. Multichaos from quasiperiodicity. *SIAM J. Appl. Dyn. Syst.*, 16(4):2196–2212, 2017.
- [16] S. Das and D. Giannakis. Koopman spectra in reproducing kernel Hilbert spaces. *Appl. Comput. Harmon. Anal.*, 49:573–607, 2020.
- [17] V. I. Paulsen and M. Raghupathi. *An Introduction to the Theory of Reproducing Kernel Hilbert Spaces*, volume 152 of *Cambridge Studies in Advanced Mathematics*. Cambridge University Press, Cambridge, 2016.
- [18] V. Paulsen. *An introduction to the theory of reproducing kernel Hilbert spaces*, 2016.
- [19] S. Das and D. Giannakis. Delay-coordinate maps and the spectra of Koopman operators. *J. Stat. Phys.*, 175:1107–1145, 2019.

- [20] D. Giannakis, S. Das, and J. Slawinska. Reproducing kernel Hilbert space compactification of unitary evolution groups. *Appl. Comput. Harmon. Anal.*, 54:75–136, 2021.
- [21] S. Das et al. Measuring quasiperiodicity. *Europhys. Lett. EPL*, 114:40005–40012, 2016.
- [22] S. Das. Lie group valued Koopman eigenfunctions, 2018.
- [23] S. Das, D. Giannakis, and E. Szekely. An information-geometric approach for feature extraction in ergodic dynamical systems, 2020.
- [24] T. Berry and D. Giannakis. Spectral exterior calculus. *Comm. Pure Appl. Math.*, 73(4):689–770, 2020.
- [25] T. Berry and J. Harlim. Variable bandwidth diffusion kernels. *Appl. Comput. Harmon. Anal.*, 40(1):68–96, 2016.
- [26] T. Berry and T. Sauer. Density estimation on manifolds with boundary. *Comput. Statist. Data Anal.*, 107:1–17, 2017.
- [27] P. Giesl and S. Hafstein. Computation and verification of Lyapunov functions. *SIAM Journal on Applied Dynamical Systems*, 14(4):1663–1698, 2015.
- [28] T. Berry, R. Cressman, Z. Gregurić-Ferenček, and T. Sauer. Time-scale separation from diffusion-mapped delay coordinates. *SIAM J. Appl. Dyn. Sys.*, 12:618–649, 2013.
- [29] D. Giannakis. Dynamics-adapted cone kernels. *SIAM J. Appl. Dyn. Sys.*, 14(2):556–608, 2015.
- [30] T. Sauer, J. A. Yorke, and M. Casdagli. Embedology. *J. Stat. Phys.*, 65(3–4):579–616, 1991.
- [31] T. Sauer. Time series prediction by using delay coordinate embedding. In A. S. Weigend and N. A. Gerhsenfeld, editors, *Time Series Prediction: Forecasting the Future and Understanding the Past*, volume 15, pages 175–193. Addison-Wesley, 2003.
- [32] T. Berry and S. Das. Learning theory for dynamical systems, 2022.
- [33] T. Buzug and G. Pfister. Comparison of algorithms calculating optimal embedding parameters for delay time coordinates. *Phys. D*, 58(1-4):127–137, 1992.
- [34] Th. Buzug and G. Pfister. Optimal delay time and embedding dimension for delay-time coordinates by analysis of the global static and local dynamical behavior of strange attractors. *Phys. rev. A*, 45(10):7073, 1992.
- [35] T. Sauer and J. Yorke. How many delay coordinates do you need? *Internat. J. Bifurcation and Chaos*, 3(03):737–744, 1993.
- [36] L. Aguirre. A nonlinear correlation function for selecting the delay time in dynamical reconstructions. *Phys. Lett. A*, 203(2-3):88–94, 1995.
- [37] R. Rahman and S. Hasan. Real-time signal queue length prediction using long short-term memory neural network. *Neural Computing and Applications*, 33(8):3311–3324, 2021.
- [38] G. Moody. A new method for detecting atrial fibrillation using rr intervals. *Computers in Cardiology*, pages 227–230, 1983.
- [39] H. Lange et al. From Fourier to Koopman: Spectral methods for long-term time series prediction. *J. Mach. Learn. Res.*, 22:41–1, 2021.

- [40] M. Williams, I. Kevrekidis, and C. Rowley. A data-driven approximation of the Koopman operator: Extending dynamic mode decomposition. *J. Nonlinear Sci.*, 25(6):1307–1346, 2015.
- [41] P. J. Schmid and J. L. Sesterhenn. Dynamic mode decomposition of numerical and experimental data. In *Bull. Amer. Phys. Soc., 61st APS meeting*, page 208, San Antonio, 2008.
- [42] Y. Kawahara. Dynamic mode decomposition with reproducing kernels for Koopman spectral analysis. In *Advances in neural information processing systems*, pages 911–919, 2016.
- [43] J. N. Kutz, X. Fu, and S. L. Brunton. Multiresolution dynamic mode decomposition. *SIAM J. Appl. Dyn. Sys.*, 15(2):713–735, 2016.
- [44] M. Korda and I. Mezić. On convergence of extended dynamic mode decomposition to the koopman operator. *J. Nonlinear Sci.*, 28(2):687–710, 2018.
- [45] Y. LeCun, Y. Bengio, and G. Hinton. Deep learning. *Nature*, 521(7553):436–444, 2015.
- [46] E. Yeung, S. Kundu, and N. Hodas. Learning deep neural network representations for koopman operators of nonlinear dynamical systems. In *2019 American Control Conference (ACC)*, pages 4832–4839. IEEE, 2019.
- [47] J. Harlim, S. Jiang, S. Liang, and H. Yang. Machine learning for prediction with missing dynamics. *J. Comput. Phys.*, 428:109922, 2021.
- [48] C. Ma, J. Wang, and E. Weinan. Model reduction with memory and the machine learning of dynamical systems. *Commun. Comput. Phys.*, 25(4):947–962, 2018.
- [49] R. Maulik et al. Time-series learning of latent-space dynamics for reduced-order model closure. *Phys D*, 405:132368, 2020.
- [50] R. Rahman and S. Hasan. Real-time signal queue length prediction using long short-term memory neural network. *Neural Comp. Appl.*, pages 1–14, 2020.
- [51] T. Berry and J. Harlim. Correcting biased observation model error in data assimilation. *Monthly Weather Review*, 145(7):2833–2853, 2017.
- [52] T. Berry, D. Giannakis, and J. Harlim. Nonparametric forecasting of low-dimensional dynamical systems. *Phys. Rev. E*, 91:032915, 2015.
- [53] R. Alexander and D. Giannakis. Operator-theoretic framework for forecasting nonlinear time series with kernel analog techniques. *Physica D*, 409:132520, 2020.
- [54] S. Das and D. Giannakis. Reproducing kernel Hilbert algebras on compact Lie groups, 2019.
- [55] Y. Lin and L. Brown. Statistical properties of the method of regularization with periodic gaussian reproducing kernel. *Ann. Stat.*, 32(4):1723–1743, 2004.
- [56] P. Hall, J. Reimann, and J. Rice. Nonparametric estimation of a periodic function. *Biometrika*, 87(3):545–557, 2000.
- [57] B. Silverman. Spline smoothing: the equivalent variable kernel method. *Ann. Stat.*, pages 898–916, 1984.
- [58] A. Tompkins and F. Ramos. Periodic kernel approximation by index set Fourier series features. In *Uncertainty in Artificial Intelligence*, pages 486–496. PMLR, 2020.